Human Molecular Genetics, 2010, Vol. 19, No. 12 **2380–2394**
doi:10.1093/hmg/ddq111
Advance Access published on March 22, 2010

Silencing ataxin-3 mitigates degeneration in a rat model of Machado–Joseph disease: no role for wild-type ataxin-3?

Sandro Alves[1,2,4], Isabel Nascimento-Ferreira[1,2], Noëlle Dufour[4,5], Raymonde Hassig[4,5], Gwennaëlle Auregan[4,5], Clévio Nóbrega[1], Emmanuel Brouillet[4,5], Philippe Hantraye[4,5], Maria C. Pedroso de Lima[1,3], Nicole Déglon[4,5] and Luís Pereira de Almeida[1,2,*]

[1]Center for Neurosciences & Cell Biology, [2]Faculty of Pharmacy and [3]Faculty of Sciences and Technology, University of Coimbra, Coimbra, Portugal, [4]CEA, Institute of Molecular Imaging (I2BM) and Molecular Imaging Research Center (MIRCen), Orsay, France and [5]CNRS URA2210, Orsay, France

Received November 8, 2009; Revised and Accepted March 16, 2010

Machado–Joseph disease or spinocerebellar ataxia type 3 (MJD/SCA3) is a fatal, autosomal dominant disorder caused by a cytosine-adenine-guanine expansion in the coding region of the *MJD1* gene. RNA interference has potential as a therapeutic approach but raises the issue of the role of wild-type ataxin-3 (WT ATX3) in MJD and of whether the expression of the wild-type protein must be maintained. To address this issue, we both overexpressed and silenced WT ATX3 in a rat model of MJD. We showed that (i) overexpression of WT ATX3 did not protect against MJD pathology, (ii) knockdown of WT ATX3 did not aggravate MJD pathology and that (iii) non-allele-specific silencing of ataxin-3 strongly reduced neuropathology in a rat model of MJD. Our findings indicate that therapeutic strategies involving non-allele-specific silencing to treat MJD patients may be safe and effective.

INTRODUCTION

Machado–Joseph disease (MJD) also known as spinocerebellar ataxia type 3 (SCA3) is a member of a family of nine neurodegenerative disorders, all clinically distinct, caused by polyglutamine (PolyQ) repeat expansions. It is the most common dominantly inherited ataxia worldwide. Patients initially present with progressive ataxia, postural instability, peripheral neuropathy, bulging eyes, ophthalmoplegia, dystonia, amyotrophy, dysarthria, nystagmus, lingual fasciculations, facial myokymia (1–3) and in some cases, parkinsonism (4–6). Neurodegeneration affects particular brain regions including the dentate nucleus, substantia nigra and pontine nuclei (2,7–9). Recent studies have also suggested the involvement of the striatum in MJD pathology (10–13). The neuropathology is caused by the expansion of a cytosine-adenine-guanine (CAG) repeat in the coding region of the *MJD1* gene which maps on chromosome 14q32.1 and encodes the ataxin-3 protein (14,15). The physiological functions of this protein are poorly understood. Several reports have suggested that ataxin-3 is involved in the ubiquitin–proteasome pathway (16–18) and that ataxin-3 has protease (19,20), deubiquitinating (21,22) and autocatalytic activities (23). Ataxin-3 is a histone-binding protein acting as a transcriptional co-repressor (24). It also interacts with DNA repair proteins (25). There are between 10 and 51 GAG repeats in healthy individuals, and consequently 10–51 glutamine residues in normal ataxin-3; MJD patients carry 55–86 repeats (26–28). Mutant ataxin-3 (MUT ATX3) promotes the formation of intranuclear aggregates (29–31) and neuronal cell loss in particular brain areas (2). In MJD patient brains, the extended CAG tract confers a toxic gain of function to MUT ATX3, together with a partial loss of function relative to wild-type ataxin-3 (WT ATX3).

There is currently no therapy available. However, a post-transcriptional gene silencing technique—RNA interference (RNAi) (32,33)—has been successfully used to degrade transcripts of disease genes efficiently, ameliorating phenotypes in several autosomal dominant neurodegenerative diseases,

*To whom correspondence should be addressed at: Center for Neurosciences & Cell Biology and Faculty of Pharmacy, University of Coimbra, Largo Marquês de Pombal, 3004-517 Coimbra, Portugal. Tel: +351 96 633 74 82; Fax: +351 239 853 409; Email: luispa@ci.uc.pt; luispa@cnc.uc.pt

such as Huntington's disease (HD) (34–38), familial forms of amyotrophic lateral sclerosis (39,40) and spinocerebellar ataxia type 1 (SCA1) (41).

RNAi has potential for the treatment of MJD, preventing neurological damage and motor deficits. Taking advantage of the presence of a single nucleotide polymorphism in linkage disequilibrium with the disease-causing CAG expansion (42), a siRNA specifically targeting the mutant allele has been developed (43). Allele-specific silencing of ataxin-3 using lentiviral vectors (LVs) significantly decreased the severity of the neuropathological abnormalities in a rat model of MJD (44). This approach is particularly attractive because the WT ATX3 allele is not targeted and consequently its normal functions are unaffected. However, this therapy would benefit ~70% of MJD patients at best (45). Whether a silencing not discriminating between wild-type and mutant alleles would be of benefit remained to be determined. A study in *Drosophila* indicated that the loss of WT ATX3 contributes to MJD pathology suggesting that the wild-type protein is neuroprotective (46). In contrast, ataxin-3 knockout mice display no major abnormalities (47).

Here, we report an investigation of the contribution of WT ATX3 to MJD. We constructed LVs allowing either the overexpression of wild-type human ataxin-3 or the silencing of endogenous ataxin-3 and studied their effects in a rat model of MJD. The absence of a role for WT ATX3 in this experimental paradigm justified the investigation of a global silencing of mutant and WT ATX3, which led to robust reduction of neurodegeneration.

RESULTS

Overexpression of WT ATX3 does not mitigate MJD neuropathology

The function of WT ATX3 in adult brain is still poorly understood. To study the contribution of WT ATX3 protein in the context of MJD and to determine whether non-allele-specific silencing can be envisaged, we used our recently developed rat model (13). In this model, the expression of mutant but not wild-type full-length ataxin-3 in the adult rat brain induces a pathology mimicking the typical features of MJD. Ubiquitinated ataxin-3 aggregates are detected 2 weeks post-infection and progressively accumulate in the nucleus of infected neurons. Neuronal dysfunction with the presence of pycnotic nuclei and loss of expression of neuronal markers is observed in the substantia nigra (tyrosine hydroxylase—TH, vesicular monoamine transporter 2) and striatum (dopamine- and cyclic AMP-regulated phosphoprotein with molecular weight 32 kDa—DARPP-32, NeuN, TH) 2 months post-injection.

To assess the contribution of WT ATX3 to MJD pathology, we co-injected LVs encoding human MUT ATX3 with WT ATX3 into the striatum of adult rats. The animals were killed 2 weeks ($n = 2$; data not shown) and 2 months ($n = 8$) after the injection and anti-ataxin-3 and anti-ubiquitin antibodies were used for immunohistochemical analysis. In all cases, a large number of ataxin-3 nuclear inclusions (Fig. 1A–C; Supplementary Material, Fig. S1A–C) were detected in the infected striata. The mutant protein accumulated in ubiquitin-positive inclusions (Fig. 1D–F; Supplementary Material, Fig. S1D–F). Quantitative analysis of ubiquitin-positive inclusions revealed no statistically significant differences between animals injected with MUT ATX3 alone (49 228 $\pm$ 3329), those co-injected with MUT ATX3 and WT ATX3 (57 272 $\pm$ 4857) and co-injected with MUT ATX3 and the control vector (49 976 $\pm$ 2518; Fig. 1D–F, M; Supplementary Material, Fig. S1D–F). Immunostaining of the striatal neuronal marker DARPP-32 showed that the depleted area in animals co-expressing WT and MUT ATX3 was larger (1.64 $\pm$ 0.12 mm^3; Fig. 1I, L and N) than that in animals injected with MUT ATX3 alone (1.31 $\pm$ 0.08 mm^3; Fig. 1H, K and N) or injected with MUT ATX3 and shRNA targeting the green fluorescent protein (shGFP) (1.38 $\pm$ 0.10 mm^3; Fig. 1G, J and N). Importantly, no significant differences in the levels of expression of both WT ATX3 ($n = 5$) and MUT ATX3 ($n = 5$) transgenic proteins were observed 2 weeks after injection of the vectors to the rat striatum (Supplementary Material, Fig. S2). This result supported the view that in this experimental model, overexpression of WT ATX3 does not suppress or reduce MUT ATX3-induced toxicity.

Efficient silencing of wild-type rat ataxin-3 *in vitro*

To study the physiological role of WT ATX3 further, we developed two shRNAs (shRatatax1 and shRatatax2) designed to specifically silence wild-type rat ataxin-3 mRNA (Fig. 2D and E). Quantitative RT–PCR analysis of 293T cells co-transfected with the shRatatax vectors and a vector expressing the wild-type rat ataxin-3 containing three interrupted CAG repeats (Fig. 2E) demonstrated robust silencing of the transcript (shRatatax1: 88.6 $\pm$ 1.4%, shRatatax2: 78.1 $\pm$ 4.6% and mixed shRatatax1/shRatatax2: 87.2 $\pm$ 3.5%, Fig. 3A). An shGFP was used as a control (Fig. 3A). Quantitative RT–PCR with LacZ oligos confirmed that the knockdown of ataxin-3 mRNA reflected the efficacy of the shRNAs and not differences in transfection efficiencies (data not shown). We verified that this silencing was associated with reduced abundance of the rat ataxin-3 protein (Fig. 3B). Co-transfection with the rat ataxin-3 plasmid and the specific shRatatax vectors led to efficient suppression as assessed by western blotting (shRatatax1: 95.5 $\pm$ 1.3%, shRatatax2: 91.2 $\pm$ 3.4% and mixed shRatatax1/shRatatax2: 95.2 $\pm$ 1.2%), whereas the control shGFP had only a small effect on the abundance of MUT ATX3 protein (12.2 $\pm$ 11%, Fig. 3B and C).

Specificity of the silencing provided by the shRNA vectors

Next, we analyzed the species selectivity of the silencing provided by shRatatax (Fig. 2D and E). 293T cells were co-transfected with human WT ATX3 and the plasmids encoding the shRatatax. An shRNA targeting a sequence conserved between the human and rat transcripts (shAtaxUNIV) and another targeting the green fluorescent protein (shGFP) were used as controls (Fig. 2C). RT–PCR and western blot analysis indicated that shRatatax1 and shGFP (Supplementary Material, Fig. S3A–C) had no effect on human ataxin-3, whereas shAtaxUNIV promoted degradation of the human ataxin-3 mRNA (Supplementary Material, Fig. S3A). To test

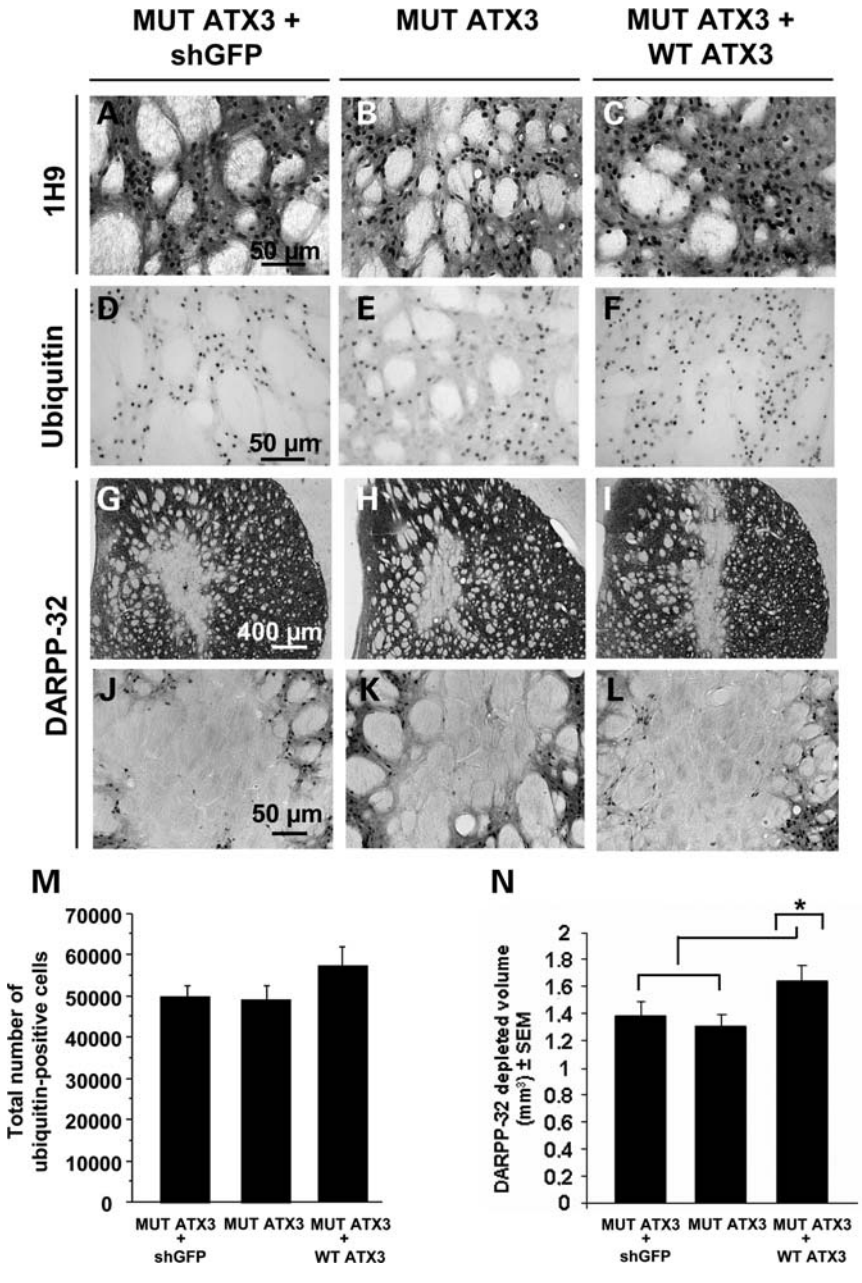

Figure 1. Effects of WT ATX3 in the brain of the adult rat model of MJD. Anti-ataxin-3 staining (1H9 antibody) revealing that LVs co-expressing MUT ATX3 and shGFP (**A**), MUT ATX3 (**B**) or co-expressing MUT ATX3 and WT ATX3 (**C**) induce the formation of ATX3-positive aggregates, a biomarker of MJD pathology, in the adult rat brain, 2 months post-injection (A, B and C). Anti-ubiquitin staining revealing ubiquitin-positive inclusions in the rat brain following overexpression of WT ATX3 (**F**) and co-injected with MUT ATX3 (**E**), and MUT ATX3 and shGFP (**D**): although there were more such inclusions following overexpression of the WT ATX3, the difference is not significant ($P > 0.05$). In all cases, a substantial loss of DARPP-32 immunoreactivity is observed in the striata infected with MUT ATX3 and shGFP (**G** and **J**), MUT ATX3 (**H** and **K**) or MUT ATX3 and WT ATX3 (**I** and **L**). The volume of the lesion in the brain of the MJD rat model, as assessed by DARPP-32 staining, was higher when WT ATX3 (I and L) was overexpressed than when MUT ATX3 (H and K) was expressed alone or co-expressed with shGFP (G and J). Quantification of the effects of WT ATX3 and shGFP expression on the absolute number (**M**) of ubiquitin-positive cells and on the DARPP-32 depleted region (**N**) is shown. Statistical significance was evaluated using Fisher's test ($^*P < 0.05$). The images shown are representative of eight sections analyzed from eight rats receiving LVs encoding MUT ATX3 alone and LVs encoding MUT ATX3 and WT ATX3 in the contralateral cerebral hemisphere. Representative images from seven rats receiving LVs encoding MUT ATX3 and shGFP are also included.

whether these shRNAs were efficient and selective in a physiologically more relevant situation, we assessed the silencing of endogenous human ataxin-3 in 293T cells by western blotting. The results confirmed the specificity of the shRNAs (Supplementary Material, Fig. S3D).

Silencing endogenous ataxin-3 in wild-type rat brain is not toxic

We then used these vectors to assess the effects of down-regulating WT ATX3 in adult rats. We co-injected LVs

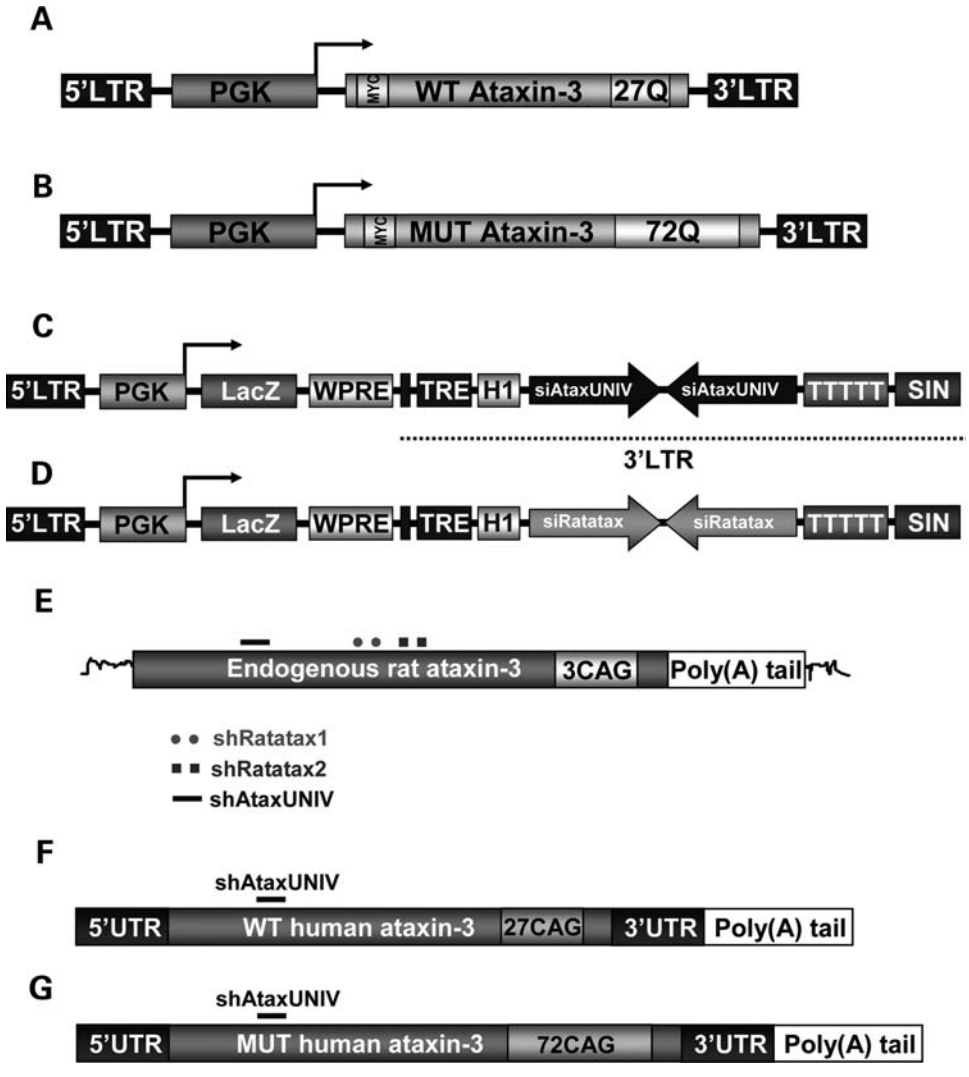

Figure 2. Scheme of the vectors used to suppress rat and human ataxin-3 (ATX3) expression by RNA interference. Schematic representation of the lentiviral constructs encoding wild-type (WT ATX3) (27 CAG repeats) (**A**) or mutant human ataxin-3 (MUT ATX3) (72 CAG repeats) (**B**) under the control of the PGK-1 promoter. (**C** and **D**) Scheme of the shAtax vectors: shRNA cassette under the control of the H1 promoter (pol III) and a separate cassette containing the LacZ reporter gene under the control of the PGK-1 promoter (used to follow expression in infected neurons). ShAtaxUNIV (C) was designed to suppress both human and rat ataxin-3, whereas shRatatax1 and shRatatax2 (D) were designed to suppress specifically rat ataxin-3. (**E**) Endogenous rat ataxin-3 mRNA is recognized by the shRatatax and shAtaxUNIV vectors, leading to its endonucleolytic cleavage. (**F** and **G**) The shAtaxUNIV vector recognizes both wild-type and mutant human ataxin-3 mRNAs, promoting their endonucleolytic cleavage and blocking the production of the encoded proteins.

encoding shRatatax1 and shRatatax2 (1:1 ratio) into the left striatum of wild-type rats ($n = 12$). As a control, the right striatum was injected with a LV encoding the shGFP. Two weeks ($n = 2$; data not shown) and 2 months ($n = 10$) post-injection, animals were killed and the expression of the LacZ reporter gene, present in the vector expressing the shRNAs, was evaluated. The β-galactosidase staining demonstrated extensive transduction of striatal neurons in both groups (Fig. 4A and B). Western blot analysis of brain lysates, collected 2 months post-injection, demonstrated that rat endogenous ataxin-3 was less abundant in the shRatatax than the control shGFP group (Fig. 3D and E). However, immunoreactivity for the neuronal markers DARPP-32 (Fig. 4C–F and K) and NeuN (Fig. 4G–J; Supplementary Material, Fig. S4) were similar in the two groups. This suggests that the decrease in WT ATX3 levels does not affect the viability of GABAergic neurons in the striatum.

Loss of WT ATX3 expression does not exacerbate MJD pathology

We next examined the effect of WT ATX3 silencing in the MJD model. The presence of WT ATX3 in inclusions and the interaction of ataxin-3 in the ubiquitin pathways raised the possibility that the wild-type protein modulates MJD pathogenesis. LVs encoding mutant human ataxin-3 and the shRatatax1/shRatatax2 were co-injected into the left striatum of rats. We used the shGFP vector as a control. MJD pathology was assessed after 2 (data not shown) and 8 weeks, corresponding to mild and severe MJD pathology, respectively (13). Ataxin-3 staining revealed the formation of ubiquitin- and ataxin-3-positive inclusions in all animals (Fig. 5C–F; Supplementary Material, Fig. S5A–D). No differences were found between the hemispheres injected with MUT ATX3

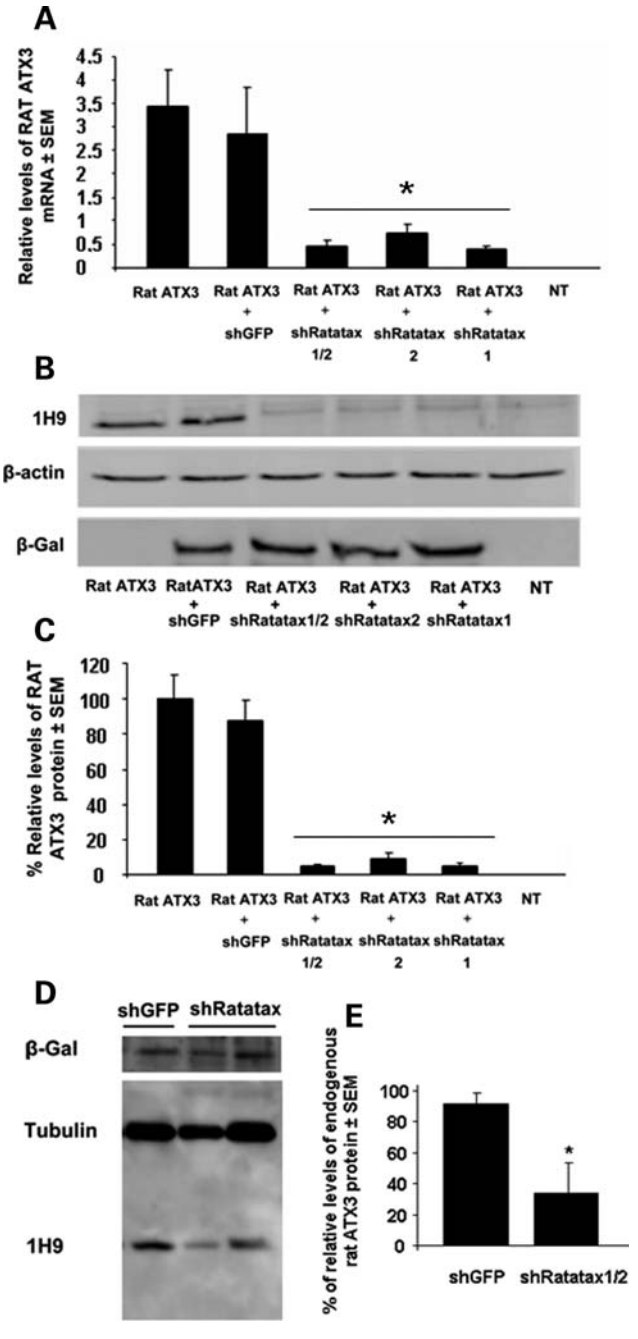

Figure 3. Robust down-regulation of rat ataxin-3 mRNA by RNA interference. (**A**) Quantitative real-time PCR analysis showing the robust silencing of rat ataxin-3 mRNA in 293T cells co-expressing wild-type rat ataxin-3 (RAT ATX3) and shRatatax1, shRatatax2 or the miss-targeted control shGFP. Endogenous β-actin mRNA was used as an internal control for the normalization and quantitative analysis of ataxin-3 mRNA 48 h after calcium-phosphate-mediated transfection. The results are expressed as the mean relative mRNA level ± SEM. (**B**) Western blot analysis of lysates of 293T cells co-transfected with the expression constructs encoding rat ataxin-3 and the shAtax vectors (48 h post-transfection; ratio of ataxin-3 to shRNA of 1:1); β-actin was used as a loading control. (**C**) Optical densitometry: the specific OD was normalized to the amount of β-actin loaded in the corresponding lane. A partition ratio was calculated and is expressed as a percentage of relative protein level ± SEM. Statistical significance was evaluated using Fisher's test ($^*P < 0.05$). (**D**) Reduced levels of ataxin-3 in rat striatum upon lentiviral-mediated gene silencing. Lysates were prepared from striatal punches 2 months after injection of LV-shRatatax or LV-shGFP. The western blot was probed simultaneously with the 1H9 and anti-tubulin antibodies. The β-galactosidase antibody allows detection of LacZ reporter gene of the shRNA. (**E**) Silencing of rat ataxin-3 mRNA reduces the amount of endogenous ataxin-3 in the rat striatum. Optical densitometry of western blot analysis of lysates of of rat brain striatum infected with LVs encoding shRatatax1/2 or the control shGFP. The specific OD was then normalized to β-tubulin in the corresponding lane. A partition ratio was calculated and is expressed as a percentage. Statistical significance was evaluated using Student's *t*-test ($P = 0.0459$, $^*P < 0.05$).

and shRatatax1/2 targeting the endogenous wild-type rat ataxin-3 (55 946 ± 3279 inclusions; Fig. 5F, K; Supplementary Material, Fig. S5D) and those injected with MUT ATX3 and shGFP (49 976 ± 2518 inclusions; Fig. 5E, K; Supplementary Material, Fig. S5C). In both cases, the β-galactosidase reporter protein co-expressed with both shRNAs co-localized with ataxin-3-positive neurons suggesting that the knockdown of endogenous rat ataxin-3 does not aggravate MJD neuropathologic signs (Supplementary Material, Fig. S6).

Similarly, the DARPP-32 depleted volume did not differ between the two groups (Fig. 5G–J and L). These results suggest that silencing wild-type endogenous ataxin-3 does not exacerbate MJD pathology; consequently, silencing both mutant and wild-type alleles in MJD patients may be a viable therapeutic option.

A universal shRNA sequence efficiently reduces expression of both human and rat ataxin-3 and prevents signs of MJD neuropathology *in vivo*

In view of these results, we further validated non-allele-specific silencing of ataxin-3 (Fig. 2C, E, F and G): RT–PCR (Fig. 6A, D and G; Supplementary Material, Fig. S3A) and western blot analysis of 293T cells transfected with shAtaxUNIV (Fig. 6B, C, E, F and H; Supplementary Material, Fig. S3B–D) demonstrated potent silencing of both human and rat ataxin-3 transcripts.

We tested the efficacy of silencing *in vivo* by co-injecting LVs encoding mutant human ataxin-3 and shAtaxUNIV into the striatum of adult rats. Western blot analysis of brain lysates showed that shAtaxUNIV, relative to the control vector (shGFP; Fig. 6I and J), efficiently reduced the levels of rat endogenous ataxin-3. In animals treated with shAtaxUNIV, the number of neurons expressing the pathogenic protein was substantially reduced (Fig. 7D and F; Supplementary Material, Figs. S7G, J and S8D). Double-staining with β-galactosidase demonstrated that neurons expressing the shRNA no longer expressed MUT ATX3 (Supplementary Material, Fig. S7I and L). As expected, the number of ubiquitin- (Fig. 7H) and ataxin-3-positive inclusions (17 376 ± 1642; an average size of 18.2 ± 0.8 μm^2; Fig. 7D, F, M and N; Supplementary Material, Fig. S7G–L) was much lower than in the control group (88 332 ± 5453; average size of 34.3 ± 1.4 μm^2; Fig. 7C, E, G, M and N; Supplementary Material, Fig. S7A–F); the DARRP-32-depleted volume was also significantly lower (0.33 ± 0.02 versus 1.53 ± 0.09 mm^3 in control animals; Fig. 7I–L and O; Supplementary Material, Fig. S8). FluoroJade B (Supplementary Material, Fig. S9B and E) and cresyl violet (Supplementary Material, Fig. S9C and F) were used to stain degenerating cells: the numbers of degenerating neurons and atrophic nuclei—leading to typical striatal shrinkage—were smaller in the shAtaxUNIV than control group (Supplementary Material, Fig. S9A and D).

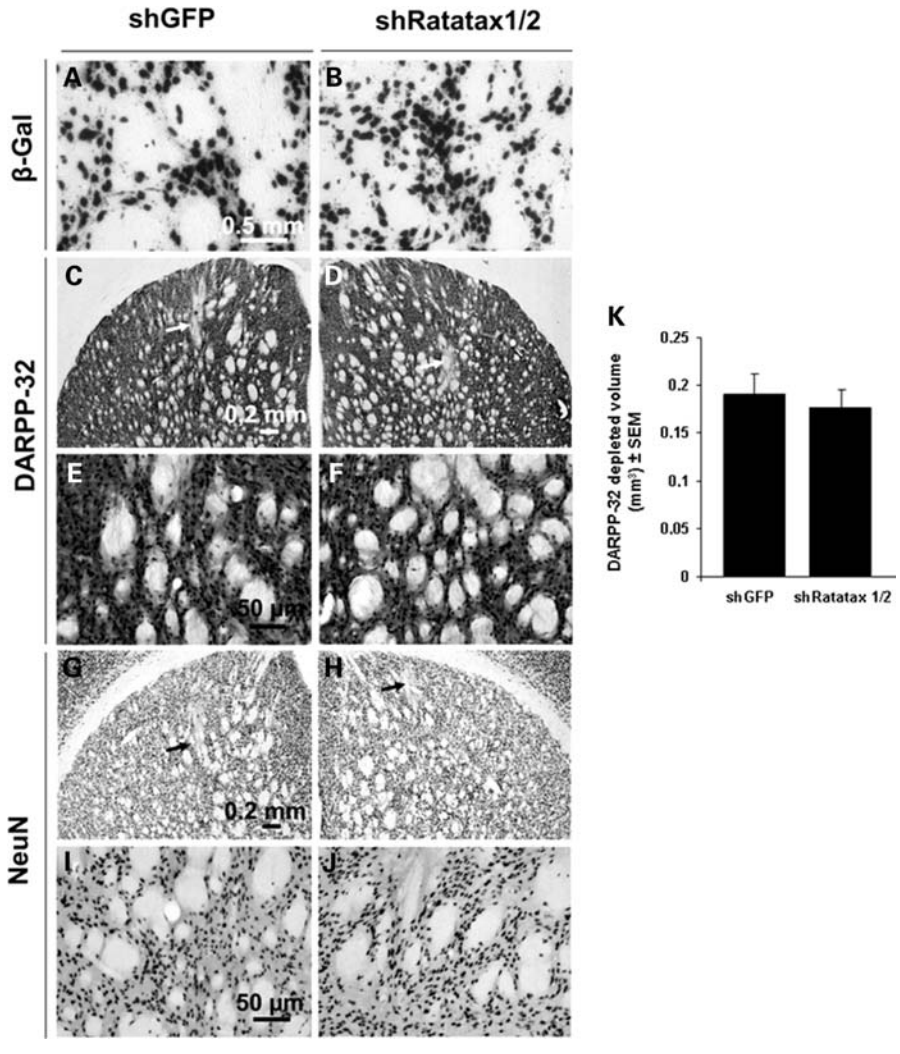

Figure 4. Endogenous ataxin-3 silencing is not toxic in wild-type rat brains. Expression in wild-type adult rat brain striata of recombinant LVs expressing the various H1 promoter-driven shGFP (**A**) or both shRatatax1 and shRatatax2 (**B**), and containing a separate PGK-LacZ cassette encoding the β-galactosidase reporter for detection of infected neurons. The H1 RNA-polymerase III promoter allows sustained expression of the shRNAs *in vivo*. Anti-DARPP-32 staining revealing no difference in the expression of DARPP-32-positive neurons 2 months after neuronal transduction with LVs encoding shRatatax1/2 (**D** and **F**) and with the miss-targeted control shGFP (**C** and **E**). Similar results were obtained for NeuN staining (**G**–**J**) demonstrating that the knockdown of endogenous rat ataxin-3 did not result in neurotoxicity at 2 months. In both cases, the arrows indicate the mechanical lesion around the needle tract area caused by the surgery. (**K**) Quantification of the DARPP-32 depleted area in the striata of adult wild-type rats injected with shGFP or shRatatax1/2 indicating the absence of lesion due to endogenous rat ataxin-3 silencing, except around the needle tract region ($P < 0.05$). The images shown are representative of eight sections analyzed from 10 rats receiving LVs encoding shRatatax1/shRatatax2 and LVs encoding the miss-targeted control shGFP in the contralateral cerebral hemisphere.

These various observations demonstrate that shAtaxUNIV substantially reduced MUT ATX3 expression, the formation of disease-associated inclusions and signs of neuropathology *in vivo*.

DISCUSSION

A key issue in the development of siRNA-based therapy for MJD is the choice between non-allele-specific and allele-specific silencing; this choice depends on whether WT ATX3 silencing is tolerated. We therefore investigated the contribution of ataxin-3 to MJD, and in particular (i) whether WT ATX3 has a neuroprotective role in the context of MJD and (ii) the effects of WT ATX3 silencing *in vivo*.

The function of the normal ataxin-3 protein has not been fully described. The normal function of ataxin-3 is linked to protein surveillance pathways (17); ataxin-3 acts as a polyubiquitin-binding protein, recruiting poly-ubiquitinated substrates through a carboxy-terminal cluster of ubiquitin interaction motifs (20,48). Ataxin-3 cleaves ubiquitin chains through its Josephin domain and thereby facilitates proteasomal degradation (21,22,49). Polyubiquitin chains linked through Lys48 were reported to be the main signal addressing ubiquitinated substrates to the proteasome (50). It was recently reported that ataxin-3 binds both Lys48-linked chains and Lys63-linked chains, but preferentially cleaves Lys63-linkages and, even more preferentially, mixed linkage polyubiquitin chains (51). This deubiquitinating activity of ataxin-3, editing complex chains, may facilitate substrate entry into the proteasome and thus efficient degradation into small peptides.

The WT ATX3 protein is found in nuclear inclusions in several PolyQ diseases (SCA1, SCA2 and Dentatorubral-pallidoluysian

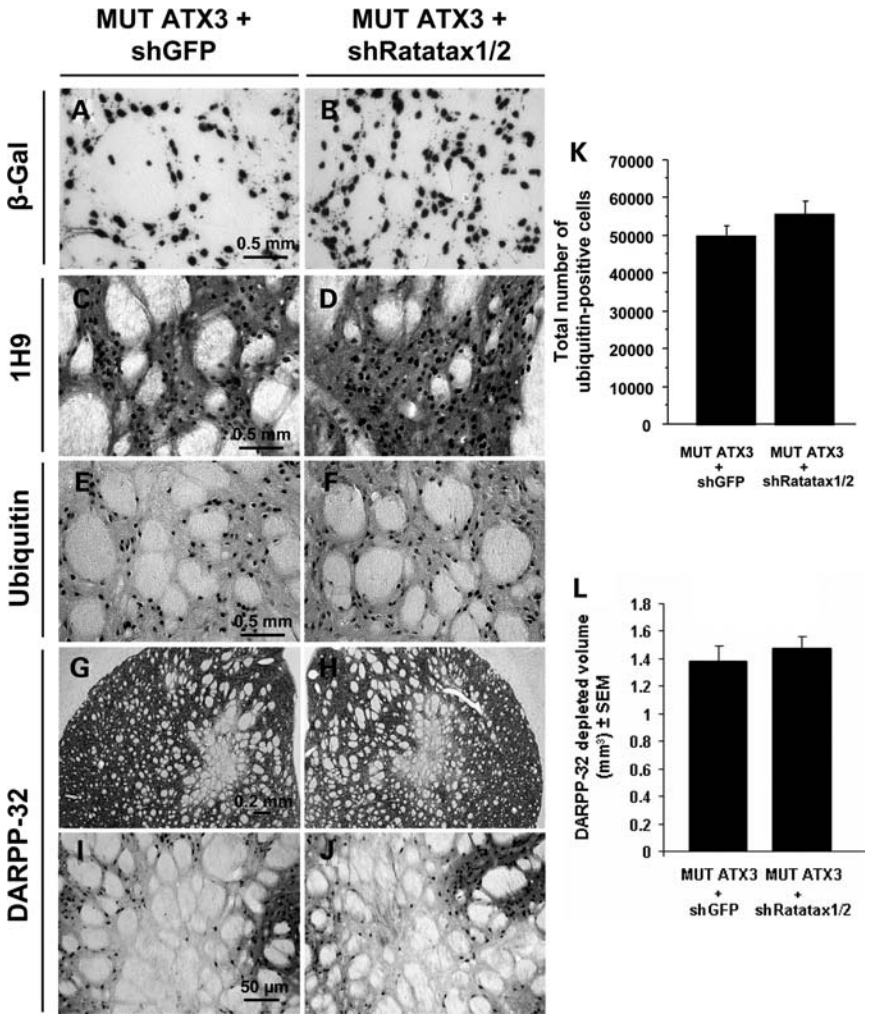

Figure 5. Silencing of endogenous rat ataxin-3 does not exacerbate the brain lesion in a rat model of MJD. (**A**) LVs encoding MUT ATX3 and shGFP (A) or both shRatatax1 and shRatatax2 (**B**) are robustly expressed in the adult rat brain striatum. The shRNA viral vectors also contain a PGK-LacZ reporter gene cassette allowing β-galactosidase expression in infected neurons to be followed. Anti-ataxin-3 staining (1H9 antibody) showing that LVs co-expressing MUT ATX3 and shGFP (A) or MUT ATX3 and shRatatax1/2, designed to specifically suppress rat ataxin-3 (B) induce the typical formation of ATX3-positive aggregates in the adult rat brain, 2 months post-injection (A, B). The animals co-injected with MUT ATX3 and shRatatax1/2 vectors show the typical accumulation of ataxin-3- and ubiquitin-positive inclusions (**D** and **F**, respectively) and a loss of DARPP-32 immunoreactivity (**H** and **J**). There were no significant differences between this group and the animals treated with the non-specific shGFP as concerns formation of ataxin-3- and of ubiquitin-positive inclusions (**C** and **E**, respectively) and DARPP-32-depleted area (**G** and **I**). Quantification of the effect of shRatatax or shGFP expression on the absolute number (**K**) of ubiquitin-positive cells and on the DARPP-32 depleted region (**L**). Statistical significance was evaluated using Student's *t*-test ($^*P < 0.05$). The images shown are representative of eight sections analyzed from seven rats receiving LVs encoding MUT ATX3 and shRatatax1/shRatatax2 and LVs encoding MUT ATX3 and shGFP in the contralateral cerebral hemisphere.

atrophy) (52) and in neuronal intranuclear hyaline inclusion disease (53); it is also found in Marinesco bodies under stressful conditions and aging in human and non-human primate brains (54–56). The depletion of ataxin-3 (by sequestration into aggregates) may therefore have deleterious consequences; alternatively, the formation of nuclear inclusions might be part of a cellular defense mechanism (57). Ataxin-3 recruitment to these inclusions raises the possibility that normal ataxin-3 and ubiquitin-mediated pathways are involved in cellular reactions against stress and misfolded proteins (55).

In the first part of the study, we analyzed the role of WT ATX3 in a rat model of MJD by co-overexpressing both wild-type and MUT ATX3. Quantitative analysis of ubiquitin-positive inclusions and the DARPP-32 depleted region revealed that WT ATX3 does not mitigate MUT ATX3-induced neurodegeneration. A study in *Drosophila* demonstrated that normal ataxin-3 suppresses the neurotoxicity of MUT ATX3 by an ubiquitin-mediated mechanism in association with the proteasome. Flies expressing MUT ATX3 were crossed with flies carrying WT ATX3. The offspring lived longer than flies expressing mutant protein and showed robust improvements in brain cortical structures. In the *Drosophila* model, WT ATX3 mediated a 2-fold reduction of MUT ATX3 levels and of the associated formation of nuclear inclusions (46). We observed no such effects by quantification of the numbers of ubiquitinated inclusions. In our data, an increase in the number of ubiquitin-positive inclusions was observed when both wild-type and MUT

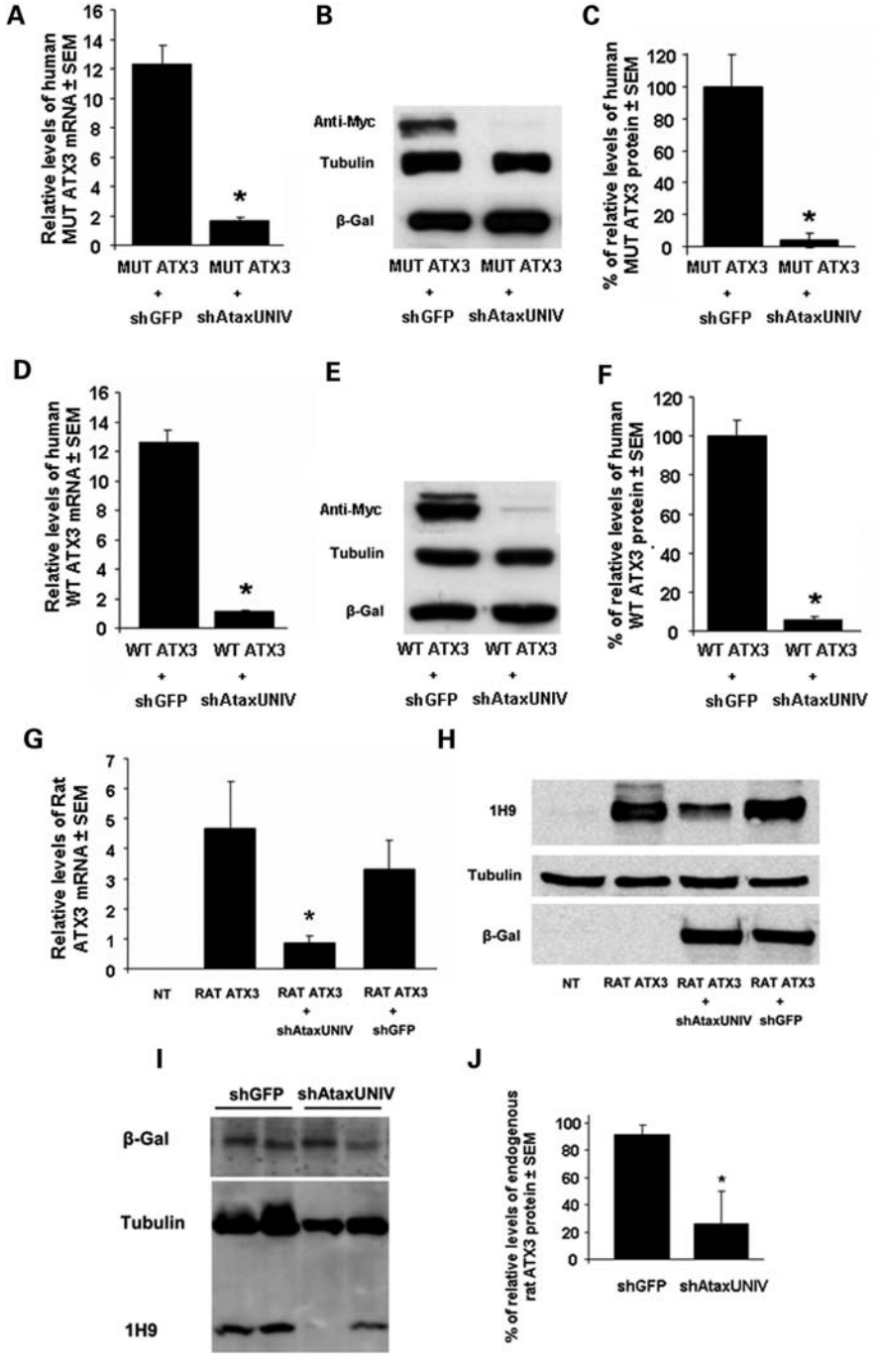

Figure 6. shAtaxUNIV efficiently silences both mutant and wild-type human ataxin-3 and rat ataxin-3. Quantitative real-time PCR analysis showing the silencing of human ATX3 mRNA in 293T cells co-expressing MUT ATX3 (**A**) or WT ATX3 (**D**) and shAtaxUNIV or shGFP. Endogenous β-actin mRNA was used as an internal control for the normalization and quantitative analysis of the ataxin-3 mRNA levels. The results are expressed as the mean relative mRNA level ± SEM. Western blot analysis of lysates of 293T cells co-transfected with the plasmid constructs encoding MUT ATX3 or WT ATX3 and the shAtaxUNIV or shGFP vectors (48 h after calcium-phosphate-mediated transfection; ratio of ATX3 to shRNA of 1:5) (**B** and **E**, respectively); (**C** and **F**) Optical densitometry: tubulin staining is shown as a loading control. The specific OD was then normalized to the amount of tubulin loaded in the corresponding lane. A partition ratio was calculated and is expressed as a percentage. Statistical significance was evaluated using Student's *t*-test ($^*P < 0.05$). RT–PCR assay demonstrating that shAtaxUNIV down-regulates rat ataxin-3 mRNA (**G**), leading to a decrease in the rat ataxin-3 protein levels (**H**), as indicated by western blotting. Statistical significance was evaluated using Fisher's *t*-test ($^*P < 0.05$). All western blots and RT–PCRs shown are representative of three or four independent experiments. (**I**) Silencing of rat ataxin-3 mRNA reduces the amount of ataxin-3 in the rat striatum. Lysates were prepared from striatal punches 2 months after injection of the universal LV-shAtaxUNIV or LV-shGFP. The western blot was probed simultaneously with 1H9 and anti-tubulin antibodies. The β-galactosidase antibody detects the immunoreactive band corresponding to the LacZ reporter gene of the shRNA. (**J**) Silencing of rat ataxin-3 mRNA reduces the amount of endogenous ataxin-3 in the rat striatum. Optical densitometry of western blot analysis of lysates of rat brain striatum infected with LV encoding shAtaxUNIV or the control shGFP. The specific OD was then normalized to the amount of tubulin loaded in the corresponding lane. A partition ratio was calculated and is expressed as a percentage. Statistical significance was evaluated using Student's *t*-test ($^*P < 0.05$). Endogenous rat ATX3 levels were normalized to β-tubulin ($P = 0.0485$).

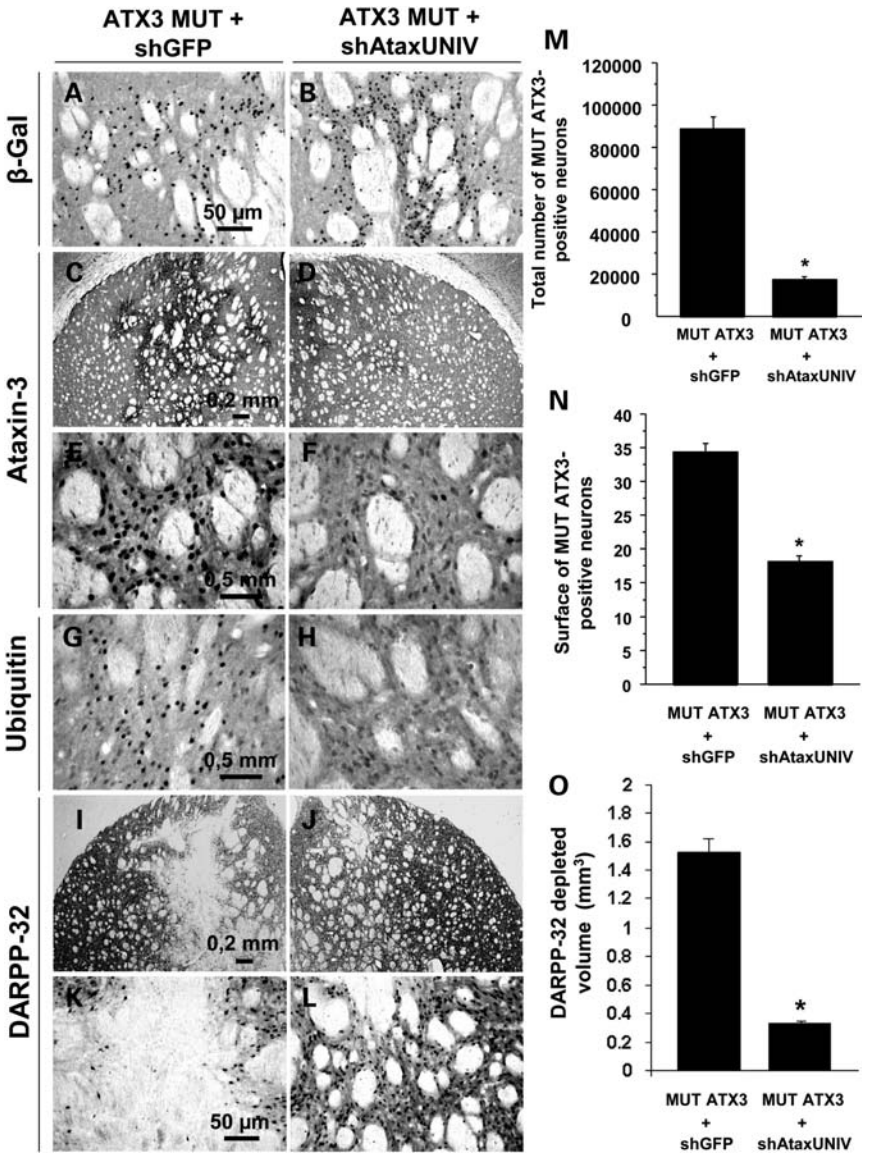

Figure 7. Silencing of mutant human ataxin-3 mediates neuroprotection in the rat striatum. Co-overexpression of MUT ATX3 and shAtaxUNIV or shGFP LV in the striatum of adult rats at 2 months. The lentiviral shRNA cassette under the control of the H1 promoter (pol III) and a second cassette containing the LacZ reporter gene are strongly expressed in the striatum (**A** and **B**). The shAtaxUNIV drastically knocks-down MUT ATX3, thus promoting a significant reduction in the amount of ataxin-3-positive aggregates (**D** and **F**) and efficiently prevents the formation of ubiquitin-positive inclusions (**H**), whereas the co-infection with shGFP shows robust expression of MUT ATX3 in neurons (**C** and **E**) and the formation of ubiquitin-positive inclusions (**G**), typical of MJD. Quantification of the effects of the various shRNAs on the absolute number (**M**) and average size (**N**) of MUT ATX3-positive aggregates ($^{*}P < 0.05$). A considerable loss of DARPP-32 immunoreactivity was observed when the striatum was infected with MUT ATX3 and the miss-targeted shGFP (**I** and **K**) but almost no DARPP-32 loss in the striatum co-infected with MUT ATX3 and shAtaxUNIV (**J** and **L**). (**O**) Quantitative analysis of the DARPP-32 depleted region in the striatum of adult rat brains co-injected with MUT ATX3 and shAtaxUNIV or shGFP LV. Statistical significance was evaluated using Student's *t*-test ($^{*}P < 0.05$). The images shown are representative of eight sections analyzed from eight rats receiving LV encoding MUT ATX3 and shAtaxUNIV or four rats receiving LV encoding MUT ATX3 and the miss-targeted control shGFP.

ATX3 are overexpressed, however, this trend was not statistically significant. Furthermore, it was associated with a larger DARPP-32-depleted region, suggesting an increased toxicity. These data can be explained by the fact that (i) MUT ATX3 associates with the nuclear matrix (ii), adopts a new conformation and (iii) may interact with WT ATX3 and promote its translocation into the nucleus, independently of the presence of an elongated glutamine expansion (58,59). This cascade of processes may well stimulate the formation of misfolded protein, thus increasing neuronal toxicity by disrupting the organization of the nucleus and affecting gene expression (60). Importantly, the *MJD1* gene is not well conserved in non-vertebrate organisms including *Drosophila*, contrary to the strong similarities of these proteins in human, rat and monkey (61); this may contribute to the discrepancy between these results. We concluded that at comparable levels of wild-type and MUT ATX3 expression, MUT ATX3 toxicity was not reduced. This does not eliminate the possibility that at higher levels of wild-type over MUT ATX3 expression, MUT ATX3 toxicity would be reduced.

In the second part of the study, we examined the effects of ataxin-3 silencing, with two shRNAs (shRatatax1 and shRatatax2) designed to specifically shut-down the expression of rat ataxin-3. Partial depletion of WT ATX3 in the striatum of adult rats was well tolerated, with no signs of toxicity for at least 2 months. These findings are in accordance with the absence of any overt abnormal phenotype in ataxin-3 knockout mice (47). They suggest some degree of redundancy in the functions of ataxin-3, such as the deubiquitinating activity that is also expressed by various other enzymes (62). *Caenorhabditis elegans* ataxin-3 knockout mutants are also viable and display no gross phenotype despite dysregulation of core sets of genes involved in the ubiquitin–proteasome system, structure/motility and signal transduction (63). These gene expression modifications may either correspond to feed-back adjustments preventing more severe effects or to dysregulation of gene expression that are not quantitatively sufficient to produce neuropathological modifications. We do not know whether similar molecular modifications occurred in our rat model, and this possibility should be further investigated.

The fact that ataxin-3 silencing is well tolerated in the brain of wild-type rats does not necessarily show that this is also the case in the context of the disease. We therefore tested the effects of rat endogenous ataxin-3 silencing in our MJD model, by simultaneously overexpressing mutant human ataxin-3 and specifically silencing rat ataxin-3 with the shRatatax vectors. Silencing rat endogenous ataxin-3 did not appear to aggravate MUT ATX3-induced toxicity and the loss of WT ATX3 did not impair the function or integrity of striatal GABAergic neurons. We then used the vector expressing the shAtaxUNIV to silence both the human MUT ATX3 and the endogenous rat ataxin-3. This non-allele-specific silencing was effective: MUT ATX3-positive inclusions declined (~80%) and DARPP-32 expression was preserved.

Our findings support the use of non-allele-specific silencing for the treatment of MJD. Additional experiments in transgenic MJD mouse models are on-going to confirm the efficacy of the shAtaxUNIV vector in rescuing the diseased phenotype particularly at the behavioral level.

This approach offers a unique opportunity to treat all MJD patients with a single product. In contrast, any allele-specific agent would be applicable to, at best, ~70% of the MJD population (42,45); at least two vectors, or even more, would have to be developed, as is the case for HD (64). Further studies are still necessary to demonstrate the safety and long-term efficacy of lentiviral-mediated administration of siRNA in transgenic MJD mice and to determine which brain areas should be targeted for optimal therapeutic benefit. But the fact that LVs (for the treatment of Parkinson's disease) (65) and siRNA have recently reached the clinic offers new hope for MJD patients.

MATERIALS AND METHODS

Generation of a cDNA encoding rat ataxin-3

Total RNA was extracted from rat cerebellum (150 mg of frozen tissue) of an adult Long Evans rat with Trizol reagent according to the manufacturer's protocol (Invitrogen, Cergy Pontoise, France). The RNA (400 ng) was treated with DNAse (Promega, Charbonnières, France) and reverse transcription was carried out as followed: 2 μM random hexamers, 16 U RNAsin (Promega, Charbonnières, France), 8 mM DTT, 200 μM dNTP, 200 U superscript II (Invitrogen, Cergy Pontoise, France) for the first-strand synthesis during 1 h at 42°C. Samples are then treated with 2 U RNAse H for 20 min at 37°C. PCR reaction was performed in thin-walled PCR tubes that contained a mixture of first-strand cDNA template, 10× PCR amplification buffer (5 μl), enhancer buffer (3 μl), 50 mM $MgSO_4$ (1 μl), 5 mM dNTPs (3 μl), 10 μM primers (1.5 μl)—RTX-1F (forward): CACCGGATCCATGGAGTCCATCTTCCACG; RTX-2R (reverse): CTCGAGCTATTTTTTCTTTCTGCTTTCAAACTG, and 2.5 U *Platinium Pfx* DNA polymerase. The final reaction volume was adjusted to 50 μl with autoclaved, distilled water. The *Pfx* enzyme, PCR buffer, enhancer buffer $MgSO_4$ solution, and four dNTPs were all purchased from Invitrogen (Invitrogen, Cergy Pontoise, France). A thermal cycler with the following cycle settings was used for amplification: 94°C for 3 min and 30 cycles of denaturation at 94°C for 30 s, annealing at 55°C for 30 s and extension at 68°C for 1.5 min for a total 30 cycles. After PCR amplification, a 5 μl aliquot of product was analyzed by electrophoresis on ethidium bromide-stained 1.5% agarose gel. The purified PCR product was then inserted into the pENTR/D-TOPO vector (Invitrogen, Cergy Pontoise, France). The sequence of the rat ataxin-3 (Rat ATX3) was confirmed by sequencing (Qiagen, Hilden, Germany). The Rat ATX3 was then transferred, with the LR clonase recombination system, into the SIN-W-PGK-CassRFA gateway vector generating the SIN-W-PGK-RAT ATX3.

Construction of shRNA plasmids

We first used two shRNAs targeting the endogenous rat ataxin-3 mRNA (Fig. 2E): shRatatax1 and shRatatax2. We also constructed a universal shRNA (shAtaxUNIV) to target human and rat ataxin-3 mRNAs simultaneously. Primers containing the sense strand, a stem-loop, the anti-sense strand, the stop codon and the nucleotides corresponding to the H1 promoter were synthesized. A shGFP was used as a control. These shRNAs were designed with the web-based tools available at Dharmacon (http://www.dharmacon.com).

shRatatax1:CTAGTTTCCAAAAAAGAACTCGCACATCTGAAATCTCTTGAATTTCAGATGTGCGAGTTCTGGGGATCTGTGGTCTCATACAGAAC; shRatatax2:CTAGTTTCCAAAAAAGATCTGGAGCGAGTCTTATCTCTTGAATAAGACTCGCTCCAGATCTGGGGATCTGTGGTCTCATACAGAAC; shAtaxUNIV:CTAGTTTCCAAAAAGAACACTGGTTTACAGTTATGACAGGAAGTAACTGTAAACCAGTGTTCGGGGATCTGTGGTCTCATACAGAAC; shGFP:CTAGTTTCCAAAAAAAGCTGACCCTGAAGTTCATCTCTTGAATGAACTTCAGGGTCAGCTTGGGGATCTGTGGTCTCATACAGAAC.

Each one of these oligomers and the primer H1-3F CACCGAACGCTGACGTCATCAACCCG were used for PCR with the plasmid pBC-H1 (pBC plasmid; Stratagene, Amsterdam, The Netherlands) containing the H1 promoter (Genbank: X16612, nucleotides 146–366) as the template. The PCR product was inserted into the pENTR/D-TOPO vector (Invitrogen, Cergy Pontoise, France). The H1-shRNA cassette was then transferred, with the LR clonase recombination system, into the SIN-CW-PGK-nls-LacZ-LTR-TRE gateway vector

which contains a tetracycline responsive element (TRE) upstream from the H1 promoter in the 3′LTR. A LacZ reporter gene was inserted downstream from the phosphoglycerate kinase 1 (PGK-1) promoter, facilitating the identification of infected neurons.

LV production

LVs encoding the various shRNAs (shRatatax1, shRatatax2, shAtaxUNIV and shGFP), mutant human ataxin-3 (MUT ATX3-72Q) and wild-type human ataxin-3 (WT ATX3-27Q) were produced in 293T cells with a four-plasmid system as previously described (66–68). The lentiviral particles were produced and resuspended in phosphate-buffered saline (PBS) containing 1% bovine serum albumin. The viral particle content of batches was determined by assaying HIV-1 p24 antigen (RETROtek, Gentaur, Paris, France). The stocks were stored at −80°C until use.

Cell culture and transfection

HEK 293T cells were cultured in DMEM (Gibco, Paisley, Scotland, UK) supplemented with 10% fetal bovine serum (Gibco, Paisley, Scotland, UK), 2 mM L-glutamine, 4500 mg/l glucose, 25 mM HEPES, 100 U/ml penicillin and 100 U/ml streptomycin (Gibco, Paisley, Scotland, UK) at 37°C in 5% CO_2/air atmosphere. One day before transfection, 293T cells were plated in six-well tissue culture dishes (Costar, NY, USA) at a density of 700 000 cells per well. Calcium-phosphate transfections were performed as follows: cells were co-transfected with the rat ataxin-3 cDNA and shRatatax 1, shRatatax2, shAtaxUNIV and shGFP (ratio 1:1). In other experiments, cells were co-transfected with SIN-W-PGK-ATX3 72Q (mutated human ataxin-3, 1 μg) or SIN-PGK-W-ATX3 27Q (WT ATX3, 1 μg) and shAtaxUNIV, shRatatax1 or shGFP (5 μg). Six hours later, the medium was removed and replaced with fresh medium. Forty-eight hours after transfection, the cell cultures were washed with cold PBS, trypsinized and harvested.

Western blotting

Harvested cells were centrifuged (1000*g*, 10 min) and the pellets were incubated on ice in lysis buffer (150 mM NaCl, 50 mM Tris-base, pH 7.4, 5 mM EDTA, 1% Triton and 0.5% protease inhibitor cocktail; Sigma) for 30 min with vortexing every 10 min. The resulting homogenates were centrifuged at 13 000*g* for 30 min at 4°C and the supernatants were stored at −80°C. Protein concentrations were determined with the Bradford protein assay (BioRad, Munich, Germany). Twenty micrograms of the protein extracts were resolved on 7.5 or 12% SDS-polyacrylamide gels. The proteins were transferred onto nitrocellulose membranes (Schleicher & Schuell Bioscience, Germany) using a Tris-Glycine (TG) 10× liquid concentrate buffer (192 mM glycine, 25 mM Tris–HCl and 20% methanol; Amresco, OH, USA). The membranes were then blocked in 5% non-fat dried milk in Tris-buffered saline containing 0.1% Tween 20 (T-Tris-buffered saline) for 1 h at room temperature (RT), followed by overnight incubation with the following primary antibodies diluted in the blocking buffer: anti-Myc tag antibody clone 4A6 (1/1000; Upstate, Cell Signalling Solutions, NY, USA); anti-β-galactosidase antibody (1:4000; Chemicon, Temecula, CA, USA), 1H9 (1:4000; Chemicon, Temecula, CA, USA), β-actin antibody (1:10 000; Sigma, Saint Louis, MO, USA) and anti-tubulin antibody (1:4000; Sigma, Saint Louis, MO,USA). Blots were washed three times (20 min per wash) and incubated with an IGg HRP-coupled secondary biotinylated goat anti-mouse or anti-rabbit antibodies (1:5000; Vector Laboratories, Burlingame, CA, USA) for 1 h at RT. After three 20 min washes, bound antibody was revealed using the Enhanced Chemiluminescence Reaction (ECL+, Amersham Pharmacia Biotech, Les Ulis, France).

Endogenous rat ataxin-3 detection by western blotting

To analyze the *in vivo* expression of human ataxin-3 after infection of the rat striatum with shRNAs, brain sections were cut in a rat slicer matrix with 2.0 mm coronal slice intervals; brain punch biopsies 2.0 mm in diameter were then obtained by dissection on dry ice of injected striatal areas from these brain sections. Brain sections were snap-frozen on dry ice and stored at −80°C. Frozen tissue was prepared for immunoblot analysis by suspension in lysis buffer (see above) and probe sonication. The samples were then frozen in liquid nitrogen and thawed three times and centrifuged for 30 min at 14 000*g* to remove insoluble material. The supernatant fraction was collected and its protein concentration was determined with the Bradford protein assay (BioRad, Munich, Germany). The blotting procedure was similar to that described above until the gel transfer process. The antibodies used were: anti-ataxin-3 antibody (1H9, 1:1000, Chemicon, Temecula, CA, USA); anti-tubulin antibody (1:10 000, Sigma, Saint Louis, MO, USA) and anti-β-galactosidase antibody (1:2000, Chemicon, Temecula, CA, USA). Blots were washed and then incubated with an alkaline phosphatase-linked secondary antibody (anti-mouse or anti-rabbit 1:20 000 in 5% non-fat dried milk). Immunoreactive bands were visualized by ECF with imaging system equipment capable of capturing high resolution digital images from chemifluorescence samples (Versadoc 3000; BioRad, Hercules, CA, USA), following incubation of the membrane with ECF reagent for 5 min.

Western blot quantification

Films were scanned, and optical density (OD) was measured using the Quantity One 1D image analysis software (version 4.4; Biorad, Hercules, CA, USA). Specific ODs were normalized to that for tubulin in experiments with total homogenates. The specific OD was then normalized according to the amount of tubulin/β-actin loaded on the corresponding lane of the same gel. A partition ratio was calculated and is expressed as a percentage.

RT–PCR analysis

Total RNAs were extracted 48 h post-transfection with Trizol reagent (Invitrogen, Cergy Pontoise, France). Real-time quantitative RT–PCR was performed in triplicate with 0.4% of

random-primed cDNAs generated from 400 ng total RNA. PCR was carried out in a 20 μl reaction volume containing Platinium SYBR Green pPCR super Mix-UDG (Invitrogen, Cergy Pontoise, France), and 10 μM of both forward (RATAX-3F: CACGAGAAACAAGAAGGCTCCC) and reverse (RATAX-4R: GCTGCTGTAAAAATGTGCGGTA GTC) primers. The ABI PRISM 7000 thermal cycler was programmed for an initial denaturation step (95°C, 2 min) followed by 40 amplification cycles (95°C, 15 s; 60°C, 1 min). The amplification rate of each target was evaluated from the cycle threshold (Ct) numbers obtained from cDNA dilutions and corrected by reference to values for human β-Actin (B-ACTIN-1F: TGAAGGTGACAGCAGTCGGTTG; B-ACTIN-2R: GGCTTTTAGGATGGCAAGGGAC) assumed to be constant. Differences between control and experimental samples were calculated using the $2^{-\Delta\Delta Ct}$ method (69). LacZ oligos were used as internal standards to assess the efficacy transfection (LacZ-1F: CCTTACTGCCGCCTGTTTTGAC; LacZ-2R: TGATGTTGAACTGGAAGTCGCC). The RT–PCR analysis was repeated with three to five samples from three to five independent transfections.

In vivo experiments

Animals. Adult male Wistar rats (Iffa Credo/Charles River, Les Oncins, France) weighing ∼200 g were used. The animals were housed in a temperature-controlled room and maintained on a 12 h light/dark cycle. Food and water were available *ad libitum*. The experiments were carried out in accordance with the European Community Council directive (86/609/EEC) for the care and use of laboratory animals.

In vivo injection with LVs. Concentrated viral stocks were thawed on ice and resuspended by repeated pipetting. The rats were anesthetized using a ketamine/xylazine solution (75 mg/kg Ketamine + 10 mg/kg xylazine, i.p.). LVs were stereotaxically injected into the striatum of rats using a 34-gauge blunt-tip needle linked to a Hamilton syringe (Hamilton, Reno, NV, USA) by a polyethylene catheter. LVs encoding human MUT ATX3 and shRNAs (shRatatax1, shRatatax2, shAtaxUNIV or shGFP) or human WT ATX3 were co-injected into adult rat striatum. The animals received a single 2.5 or 5 μl injection of lentivirus (particle content of the injected preparation was equivalent to 200 000 ng of p24/ml or 250 000 ng of p24/ml) in each side at the following coordinates: 0.5 mm rostral to bregma, ±3 mm lateral to midline and 5 mm ventral from the skull surface, with the mouth bar set at zero. The viral suspensions were injected at 0.2 μl/min by means of an automatic injector (Stoelting Co., Wood Dale, USA) and the needle was left in place for an additional 5 min. The skin was closed using wound chip autoclips (Phymep, Paris, France).

Histological processing

Tissue preparation. Two weeks or 2 months post-lentiviral injection, the animals were killed by sodium pentobarbital overdose and were transcardially perfused with a phosphate solution followed by fixation with 4% paraformaldehyde (PAF, Fluka, Sigma, Buchs, Switzerland) and 10% picric acid. The brains were removed and post-fixed in 4% PAF and 10% picric acid for 24 h and finally cryoprotected in 25% sucrose/0.1 M phosphate buffer for 48 h. The brains were frozen and 25 μm coronal sections were cut on a sliding microtome (Cryocut 1800, Leica Microsystems AG, Glattbrugg, Switzerland) at −20°C. Slices throughout the entire striatum were collected and stored in 48-well trays (Corning Inc., NY, USA) as free-floating sections in PBS supplemented with 0.12 μM sodium azide. The trays were stored at 4°C until immunohistochemical processing.

Primary antibodies. Striatal sections from injected rats were processed with the following primary antibodies: a rabbit polyclonal anti-ataxin-3 antibody, kindly provided by Dr Henry L. Paulson, a mouse monoclonal anti-ataxin-3 antibody (1H9) (Chemicon, Temecula, CA, USA), recognizing the human ataxin-3 fragment F112-L249; a rabbit polyclonal anti-ubiquitin antibody (Dakocytomation, Zug, Switzerland); a rabbit polyclonal anti-DARPP-32 (Chemicon, Temecula, CA, USA) antibody recognizing the DARPP-32; a rabbit polyclonal anti-β-galactosidase (Chemicon, Temecula, CA, USA) antibody and a mouse monoclonal anti-NeuN antibody (Chemicon, Temecula, CA,USA).

Immunohistochemical procedure. The immunohistochemical procedure was initiated by quenching endogenous peroxidase by incubating free-floating sections for 1 h at 37°C in PBS containing 0.1% diphenylhydrazine. The sections were incubated at RT for 1 h in PBS/0.1% Triton X-100 (or PBS/0.02% Triton X-100 for the anti-ubiquitin antibody) containing 10% Normal Goat Serum (NGS, Gibco), and then with the appropriate antibodies: 1H9 [1:5000; overnight (O/N) 4°C], anti-ataxin-3 antibody, kindly provided by Dr Henry L. Paulson (1:5000; O/N 4°C), anti-ubiquitin (1:1000; O/N 4°C), DARPP-32 (1:5000, O/N 4°C), NeuN (1:2000, O/N 4°C) and β-galactosidase (1:5000, O/N 4°C) diluted in PBS/0.1% Triton X-100 and 10% NGS solution. After three washings, the sections were incubated with the corresponding biotinylated secondary antibody (1:200; Vector Laboratories Inc., CA, USA) diluted in PBS/0.1% Triton X-100 and 10% NGS for 2 h at RT. After three washes, bound antibodies were visualized by the ABC amplification system (Vectastain ABC kit, Vector Laboratories, West Grove, USA) and 3,3′-diaminobenzidine tetrahydrochloride (peroxidase substrate kit, DAB, Vector Laboratories, CA, USA) as the substrate. The sections were mounted, dehydrated by passing twice through ethanol and toluol solutions, and coverslipped with Eukitt® (O. Kindler GmbH & CO, Freiburg, Germany).

Double stainings for Ataxin-3/DARPP-32, Ataxin-3/β-galactosidase and NeuN/β-galactosidase were also performed. Free-floating sections were incubated at RT for 1 h in PBS/0.1% Triton X-100 containing 10% (NGS, Gibco), and then in the blocking solution containing the appropriate antibodies: 1H9 (1:5000; O/N 4°C), DARPP-32 (1:5000, O/N 4°C), NeuN (1:2000, O/N 4°C) and β-galactosidase (1:5000, O/N 4°C). After three washes, the sections were incubated with the corresponding secondary antibodies coupled to fluorophores (1:200; Molecular Probes, OR, USA) diluted in PBS/0.1% Triton X-100 and 10% NGS for 2 h at RT. The

sections were washed three times and then mounted in Fluorsave Reagent (Calbiochem, Germany) on microscope slides.

Cresyl violet staining. Premounted sections were stained with cresyl violet for 2 min, differentiated in acetate buffer pH 3.8–4 (2.72% sodium acetate and 1.2% acetic acid; 1:4 v/v), dehydrated by passing twice through ethanol and toluol solutions, and mounted onto microscope slides with Eukitt® (O. Kindler GmbH & CO).

FluoroJade B staining. We stained striatal sections with FluoroJade B (Chemicon, Temecula, CA, USA), an anionic fluorescein derivative which stains neurons undergoing degeneration. The sections were first washed in water and then mounted on sylanized glass slides, dehydrated and stained according to the supplier's manual (70). Brightfield and fluorescent images were acquired digitally on an Axioskop 2 Plus (Zeiss, Germany) with the Axiovision software 4.2. All photographs for comparison were taken under identical conditions of image acquisition, and all adjustments of brightness and contrast were applied uniformly to all images.

Evaluation of the volume of DARPP-32 depleted region

The quantitative analysis was performed as previously described (13).

Analysis of ataxin-3 aggregate-positive signals

Cell counts and morphometric analysis of inclusions were performed as previously described with minor modifications (71,72). Coronal sections constituting complete rostrocaudal sampling (one of eight sections) of the striatum (73) were scanned with a 10× objective using a Zeiss (Oberkochen, Germany) Axioplan 2 imaging microscope motorized for *X*, *Y* and *Z* displacements using an image acquisition and analysis system (Morphostar V 6.0; IMSTAR, Paris, France). Areas analyzed in the striatum encompassed the entire region showing MUT ATX3 aggregates as revealed by the anti-ataxin-3 antibody. This represented, on average, 100 contiguous digitized images per section. Image pixels were 0.8 μm × 0.8 μm. Section lighting was similar for all acquisitions and was automatically corrected using blank images. Images were automatically segmented for the quantification of dark objects (aggregates/inclusions), using the same parameters defining light intensity threshold, and object size and shape filters. With this procedure, all inclusions with an apparent cross-sectional area greater than 3 μm^2 were reliably detected. For all images, objects touching one of the *X* or *Y* borders of the fields of view were not counted. For each animal, the estimated total number of inclusions (N_e) was calculated as $N_e = (N_s)/S_f$, where N_s is the number of inclusions detected in all sections and S_f is the rostrocaudal sampling fraction (1/8). As inclusions in striatal neurons were round on average (mean rotundity index >0.90) with an isotropic orientation in the striatum, the number of raw cell counts was corrected using the Abercrombie factor (74). This factor was calculated using the formula, $A = N/N + h$, where N is the section thickness and h the mean object height that was estimated for each experimental group by morphometric analysis of segmented objects (shGFP, 6.61 μm; shAtaxU-NIV, 4.81 μm). The corrected total number of inclusions (N_c) was calculated as $N_c = A \times N_e$.

Cell count analysis of ubiquitinated inclusions

Counts of cells with inclusions were performed as described above with some modifications. Coronal sections constituting complete rostrocaudal sampling (one of eight sections) of the striatum (73) were scanned with a 20× objective using a Zeiss Axiovert 200 M imaging microscope Zeiss (Zeiss, Germany) motorized for *X*, *Y* and *Z* displacements using the image acquisition and analysis system PALM Robot Software (version 4.0). Areas analyzed in the striatum encompassed the entire region showing ubiquitin aggregates as revealed by the anti-ubiquitin antibody. This represented, on average, 50 contiguous digitized images per section. Section lighting was similar for all acquisitions and was automatically corrected using blank images. Images were automatically segmented for the quantification of dark objects (aggregates/inclusions), using the same parameters defining the light intensity threshold. For all images, objects touching one of the *X* or *Y* borders of the fields of view were not counted. For each animal, the estimated total number of inclusions (N_e) was calculated as $N_e = (N_s)/S_f$, where N_s is the number of inclusions detected in all sections and S_f is the rostrocaudal sampling fraction (1/8).

Data analysis

All quantifications are expressed as mean ± SEM. Statistical analysis involved one-way analysis of variance followed by a PLSD de Fisher *post hoc* test (StatView 4.0, version 3.2.6; Aladdin Systems) or the Student's *t*-test. The significance thresholds were set at $P < 0.05$.

SUPPLEMENTARY MATERIAL

Supplementary Material is available at *HMG* online.

ACKNOWLEDGEMENTS

We thank Philippe Colin and Luísa Cortes for expert technical assistance and Dr Henry L. Paulson for providing the anti-ataxin-3 antibody.

Conflict of Interest statement. None declared.

FUNDING

We acknowledge funding from the Portuguese Foundation for Science and Technology (FCT—POCI/SAU-MMO/56055/2004, PTDC/SAU-FCF/70384/2006; L.P.A.); the National Ataxia Foundation (Grant #8 04/05; USA; L.P.A.) and the Commissariat à l'Energie Atomique (CEA, N.D.). Sandro Alves and Isabel Nascimento-Ferreira were supported by the Portuguese Foundation for Science and Technology (Fellowships SFRH/BD/12675/2003 and SFRH/BD/29479/2006).

REFERENCES

1. Takiyama, Y., Oyanagi, S., Kawashima, S., Sakamoto, H., Saito, K., Yoshida, M., Tsuji, S., Mizuno, Y. and Nishizawa, M. (1994) A clinical and pathologic study of a large Japanese family with Machado–Joseph disease tightly linked to the DNA markers on chromosome 14q. *Neurology*, **44**, 1302–1308.
2. Sudarsky, L. and Coutinho, P. (1995) Machado–Joseph disease. *Clin. Neurosci.*, **3**, 17–22.
3. Rosenberg, R.N. (1992) Machado–Joseph disease: an autosomal dominant motor system degeneration. *Mov. Disord.*, **7**, 193–203.
4. Subramony, S.H., Hernandez, D., Adam, A., Smith-Jefferson, S., Hussey, J., Gwinn-Hardy, K., Lynch, T., McDaniel, O., Hardy, J., Farrer, M. and Singleton, A. (2002) Ethnic differences in the expression of neurodegenerative disease: Machado–Joseph disease in Africans and Caucasians. *Mov. Disord.*, **17**, 1068–1071.
5. Gwinn-Hardy, K., Singleton, A., O'Suilleabhain, P., Boss, M., Nicholl, D., Adam, A., Hussey, J., Critchley, P., Hardy, J. and Farrer, M. (2001) Spinocerebellar ataxia type 3 phenotypically resembling parkinson disease in a black family. *Arch. Neurol.*, **58**, 296–299.
6. Lu, C.S., Chang, H.C., Kuo, P.C., Liu, Y.L., Wu, W.S., Weng, Y.H., Yen, T.C. and Chou, Y.H. (2004) The parkinsonian phenotype of spinocerebellar ataxia type 3 in a Taiwanese family. *Parkinsonism Relat. Disord.*, **10**, 369–373.
7. Durr, A., Stevanin, G., Cancel, G., Duyckaerts, C., Abbas, N., Didierjean, O., Chneiweiss, H., Benomar, A., Lyon-Caen, O., Julien, J. *et al.* (1996) Spinocerebellar ataxia 3 and Machado–Joseph disease: clinical, molecular, and neuropathological features. *Ann. Neurol.*, **39**, 490–499.
8. Paulson, H.L., Das, S.S., Crino, P.B., Perez, M.K., Patel, S.C., Gotsdiner, D., Fischbeck, K.H. and Pittman, R.N. (1997) Machado–Joseph disease gene product is a cytoplasmic protein widely expressed in brain. *Ann. Neurol.*, **41**, 453–462.
9. Fowler, H.L. (1984) Machado–Joseph-Azorean disease. A 10-year study. *Arch. Neurol.*, **41**, 921–925.
10. Yen, T.C., Lu, C.S., Tzen, K.Y., Wey, S.P., Chou, Y.H., Weng, Y.H., Kao, P.F. and Ting, G. (2000) Decreased dopamine transporter binding in Machado–Joseph disease. *J. Nucl. Med.*, **41**, 994–998.
11. Yen, T.C., Tzen, K.Y., Chen, M.C., Chou, Y.H., Chen, R.S., Chen, C.J., Wey, S.P., Ting, G. and Lu, C.S. (2002) Dopamine transporter concentration is reduced in asymptomatic Machado–Joseph disease gene carriers. *J. Nucl. Med.*, **43**, 153–159.
12. Taniwaki, T., Sakai, T., Kobayashi, T., Kuwabara, Y., Otsuka, M., Ichiya, Y., Masuda, K. and Goto, I. (1997) Positron emission tomography (PET) in Machado–Joseph disease. *J. Neurol. Sci.*, **145**, 63–67.
13. Alves, S., Regulier, E., Nascimento-Ferreira, I., Hassig, R., Dufour, N., Koeppen, A., Carvalho, A.L., Simoes, S., Pedroso de Lima, M.C., Brouillet, E. *et al.* (2008) Striatal and nigral pathology in a lentiviral rat model of Machado–Joseph disease. *Hum. Mol. Genet.*, **17**, 2071–2083.
14. Kawaguchi, Y., Okamoto, T., Taniwaki, M., Aizawa, M., Inoue, M., Katayama, S., Kawakami, H., Nakamura, S., Nishimura, M., Akiguchi, I. *et al.* (1994) CAG expansions in a novel gene for Machado–Joseph disease at chromosome 14q32.1. *Nat. Genet.*, **8**, 221–228.
15. Matilla, T., McCall, A., Subramony, S.H. and Zoghbi, H.Y. (1995) Molecular and clinical correlations in spinocerebellar ataxia type 3 and Machado–Joseph disease. *Ann. Neurol.*, **38**, 68–72.
16. Wang, G., Ide, K., Nukina, N., Goto, J., Ichikawa, Y., Uchida, K., Sakamoto, T. and Kanazawa, I. (1997) Machado–Joseph disease gene product identified in lymphocytes and brain. *Biochem. Biophys. Res. Commun.*, **233**, 476–479.
17. Chai, Y., Berke, S.S., Cohen, R.E. and Paulson, H.L. (2004) Poly-ubiquitin binding by the polyglutamine disease protein ataxin-3 links its normal function to protein surveillance pathways. *J. Biol. Chem.*, **279**, 3605–3611.
18. Doss-Pepe, E.W., Stenroos, E.S., Johnson, W.G. and Madura, K. (2003) Ataxin-3 interactions with rad23 and valosin-containing protein and its associations with ubiquitin chains and the proteasome are consistent with a role in ubiquitin-mediated proteolysis. *Mol. Cell. Biol.*, **23**, 6469–6483.
19. Scheel, H., Tomiuk, S. and Hofmann, K. (2003) Elucidation of ataxin-3 and ataxin-7 function by integrative bioinformatics. *Hum. Mol. Genet.*, **12**, 2845–2852.
20. Burnett, B., Li, F. and Pittman, R.N. (2003) The polyglutamine neurodegenerative protein ataxin-3 binds polyubiquitylated proteins and has ubiquitin protease activity. *Hum. Mol. Genet.*, **12**, 3195–3205.
21. Mao, Y., Senic-Matuglia, F., Di Fiore, P.P., Polo, S., Hodsdon, M.E. and De Camilli, P. (2005) Deubiquitinating function of ataxin-3: insights from the solution structure of the Josephin domain. *Proc. Natl. Acad. Sci. USA*, **102**, 12700–12705.
22. Nicastro, G., Menon, R.P., Masino, L., Knowles, P.P., McDonald, N.Q. and Pastore, A. (2005) The solution structure of the Josephin domain of ataxin-3: structural determinants for molecular recognition. *Proc. Natl. Acad. Sci. USA*, **102**, 10493–10498.
23. Mauri, P.L., Riva, M., Ambu, D., De Palma, A., Secundo, F., Benazzi, L., Valtorta, M., Tortora, P. and Fusi, P. (2006) Ataxin-3 is subject to autolytic cleavage. *Febs. J.*, **273**, 4277–4286.
24. Li, F., Macfarlan, T., Pittman, R.N. and Chakravarti, D. (2002) Ataxin-3 is a histone-binding protein with two independent transcriptional corepressor activities. *J. Biol. Chem.*, **277**, 45004–45012.
25. Wang, G., Sawai, N., Kotliarova, S., Kanazawa, I. and Nukina, N. (2000) Ataxin-3, the MJD1 gene product, interacts with the two human homologs of yeast DNA repair protein RAD23, HHR23A and HHR23B. *Hum. Mol. Genet.*, **9**, 1795–1803.
26. Cummings, C.J. and Zoghbi, H.Y. (2000) Fourteen and counting: unraveling trinucleotide repeat diseases. *Hum. Mol. Genet.*, **9**, 909–916.
27. Cummings, C.J. and Zoghbi, H.Y. (2000) Trinucleotide repeats: mechanisms and pathophysiology. *Annu. Rev. Genomics Hum. Genet.*, **1**, 281–328.
28. Maciel, P., Costa, M.C., Ferro, A., Rousseau, M., Santos, C.S., Gaspar, C., Barros, J., Rouleau, G.A., Coutinho, P. and Sequeiros, J. (2001) Improvement in the molecular diagnosis of Machado–Joseph disease. *Arch. Neurol.*, **58**, 1821–1827.
29. Schmidt, T., Landwehrmeyer, G.B., Schmitt, I., Trottier, Y., Auburger, G., Laccone, F., Klockgether, T., Volpel, M., Epplen, J.T., Schols, L. and Riess, O. (1998) An isoform of ataxin-3 accumulates in the nucleus of neuronal cells in affected brain regions of SCA3 patients. *Brain Pathol.*, **8**, 669–679.
30. Trottier, Y., Cancel, G., An-Gourfinkel, I., Lutz, Y., Weber, C., Brice, A., Hirsch, E. and Mandel, J.L. (1998) Heterogeneous intracellular localization and expression of ataxin-3. *Neurobiol. Dis.*, **5**, 335–347.
31. Cancel, G., Abbas, N., Stevanin, G., Durr, A., Chneiweiss, H., Neri, C., Duyckaerts, C., Penet, C., Cann, H.M., Agid, Y. *et al.* (1995) Marked phenotypic heterogeneity associated with expansion of a CAG repeat sequence at the spinocerebellar ataxia 3/Machado–Joseph disease locus. *Am. J. Hum. Genet.*, **57**, 809–816.
32. Mello, C.C. and Conte, D. Jr (2004) Revealing the world of RNA interference. *Nature*, **431**, 338–342.
33. Elbashir, S.M., Harborth, J., Lendeckel, W., Yalcin, A., Weber, K. and Tuschl, T. (2001) Duplexes of 21-nucleotide RNAs mediate RNA interference in cultured mammalian cells. *Nature*, **411**, 494–498.
34. Machida, Y., Okada, T., Kurosawa, M., Oyama, F., Ozawa, K. and Nukina, N. (2006) rAAV-mediated shRNA ameliorated neuropathology in Huntington disease model mouse. *Biochem. Biophys. Res. Commun.*, **343**, 190–197.
35. DiFiglia, M., Sena-Esteves, M., Chase, K., Sapp, E., Pfister, E., Sass, M., Yoder, J., Reeves, P., Pandey, R.K., Rajeev, K.G. *et al.* (2007) Therapeutic silencing of mutant huntingtin with siRNA attenuates striatal and cortical neuropathology and behavioral deficits. *Proc. Natl. Acad. Sci. USA*, **104**, 17204–17209.
36. Harper, S.Q., Staber, P.D., He, X., Eliason, S.L., Martins, I.H., Mao, Q., Yang, L., Kotin, R.M., Paulson, H.L. and Davidson, B.L. (2005) RNA interference improves motor and neuropathological abnormalities in a Huntington's disease mouse model. *Proc. Natl. Acad. Sci. USA*, **102**, 5820–5825.
37. Rodriguez-Lebron, E., Denovan-Wright, E.M., Nash, K., Lewin, A.S. and Mandel, R.J. (2005) Intrastriatal rAAV-mediated delivery of anti-huntingtin shRNAs induces partial reversal of disease progression in R6/1 Huntington's disease transgenic mice. *Mol. Ther.*, **12**, 618–633.
38. Franich, N.R., Fitzsimons, H.L., Fong, D.M., Klugmann, M., During, M.J. and Young, D. (2008) AAV vector-mediated RNAi of mutant huntingtin expression is neuroprotective in a novel genetic rat model of Huntington's disease. *Mol. Ther.*, **16**, 947–956.
39. Ralph, G.S., Radcliffe, P.A., Day, D.M., Carthy, J.M., Leroux, M.A., Lee, D.C., Wong, L.F., Bilsland, L.G., Greensmith, L., Kingsman, S.M. *et al.* (2005) Silencing mutant SOD1 using RNAi protects against neurodegeneration and extends survival in an ALS model. *Nat. Med.*, **11**, 429–433.

40. Raoul, C., Abbas-Terki, T., Bensadoun, J.C., Guillot, S., Haase, G., Szulc, J., Henderson, C.E. and Aebischer, P. (2005) Lentiviral-mediated silencing of SOD1 through RNA interference retards disease onset and progression in a mouse model of ALS. *Nat. Med.*, **11**, 423–428.
41. Xia, H., Mao, Q., Eliason, S.L., Harper, S.Q., Martins, I.H., Orr, H.T., Paulson, H.L., Yang, L., Kotin, R.M. and Davidson, B.L. (2004) RNAi suppresses polyglutamine-induced neurodegeneration in a model of spinocerebellar ataxia. *Nat. Med.*, **10**, 816–820.
42. Gaspar, C., Lopes-Cendes, I., DeStefano, A.L., Maciel, P., Silveira, I., Coutinho, P., MacLeod, P., Sequeiros, J., Farrer, L.A. and Rouleau, G.A. (1996) Linkage disequilibrium analysis in Machado–Joseph disease patients of different ethnic origins. *Hum. Genet.*, **98**, 620–624.
43. Miller, V.M., Xia, H., Marrs, G.L., Gouvion, C.M., Lee, G., Davidson, B.L. and Paulson, H.L. (2003) Allele-specific silencing of dominant disease genes. *Proc. Natl. Acad. Sci. USA*, **100**, 7195–7200.
44. Alves, S., Nascimento-Ferreira, I., Auregan, G., Hassig, R., Dufour, N., Brouillet, E., Pedroso de Lima, M.C., Hantraye, P., Pereira de Almeida, L. and Deglon, N. (2008) Allele-specific RNA silencing of mutant ataxin-3 mediates neuroprotection in a rat model of Machado–Joseph disease. *PLoS ONE*, **3**, e3341.
45. Gaspar, C., Lopes-Cendes, I., Hayes, S., Goto, J., Arvidsson, K., Dias, A., Silveira, I., Maciel, P., Coutinho, P., Lima, M. *et al.* (2001) Ancestral origins of the Machado–Joseph disease mutation: a worldwide haplotype study. *Am. J. Hum. Genet.*, **68**, 523–528.
46. Warrick, J.M., Morabito, L.M., Bilen, J., Gordesky-Gold, B., Faust, L.Z., Paulson, H.L. and Bonini, N.M. (2005) Ataxin-3 suppresses polyglutamine neurodegeneration in *Drosophila* by a ubiquitin-associated mechanism. *Mol. Cell.*, **18**, 37–48.
47. Schmitt, I., Linden, M., Khazneh, H., Evert, B.O., Breuer, P., Klockgether, T. and Wuellner, U. (2007) Inactivation of the mouse Atxn3 (ataxin-3) gene increases protein ubiquitination. *Biochem. Biophys. Res. Commun.*, **362**, 734–739.
48. Donaldson, K.M., Li, W., Ching, K.A., Batalov, S., Tsai, C.C. and Joazeiro, C.A. (2003) Ubiquitin-mediated sequestration of normal cellular proteins into polyglutamine aggregates. *Proc. Natl. Acad. Sci. USA*, **100**, 8892–8897.
49. Boeddrich, A., Gaumer, S., Haacke, A., Tzvetkov, N., Albrecht, M., Evert, B.O., Muller, E.C., Lurz, R., Breuer, P., Schugardt, N. *et al.* (2006) An arginine/lysine-rich motif is crucial for VCP/p97-mediated modulation of ataxin-3 fibrillogenesis. *Embo. J.*, **25**, 1547–1558.
50. Thrower, J.S., Hoffman, L., Rechsteiner, M. and Pickart, C.M. (2000) Recognition of the polyubiquitin proteolytic signal. *Embo. J.*, **19**, 94–102.
51. Winborn, B.J., Travis, S.M., Todi, S.V., Scaglione, K.M., Xu, P., Williams, A.J., Cohen, R.E., Peng, J. and Paulson, H.L. (2008) The deubiquitinating enzyme ataxin-3, a polyglutamine disease protein, edits Lys63 linkages in mixed linkage ubiquitin chains. *J. Biol. Chem.*, **283**, 26436–26443.
52. Uchihara, T., Fujigasaki, H., Koyano, S., Nakamura, A., Yagishita, S. and Iwabuchi, K. (2001) Non-expanded polyglutamine proteins in intranuclear inclusions of hereditary ataxias–triple-labeling immunofluorescence study. *Acta. Neuropathol.*, **102**, 149–152.
53. Takahashi, J., Tanaka, J., Arai, K., Funata, N., Hattori, T., Fukuda, T., Fujigasaki, H. and Uchihara, T. (2001) Recruitment of nonexpanded polyglutamine proteins to intranuclear aggregates in neuronal intranuclear hyaline inclusion disease. *J. Neuropathol. Exp. Neurol.*, **60**, 369–376.
54. Fujigasaki, H., Uchihara, T., Koyano, S., Iwabuchi, K., Yagishita, S., Makifuchi, T., Nakamura, A., Ishida, K., Toru, S., Hirai, S. *et al.* (2000) Ataxin-3 is translocated into the nucleus for the formation of intranuclear inclusions in normal and Machado–Joseph disease brains. *Exp. Neurol.*, **165**, 248–256.
55. Fujigasaki, H., Uchihara, T., Takahashi, J., Matsushita, H., Nakamura, A., Koyano, S., Iwabuchi, K., Hirai, S. and Mizusawa, H. (2001) Preferential recruitment of ataxin-3 independent of expanded polyglutamine: an immunohistochemical study on Marinesco bodies. *J. Neurol. Neurosurg. Psychiatry*, **71**, 518–520.
56. Kettner, M., Willwohl, D., Hubbard, G.B., Rub, U., Dick, E.J. Jr, Cox, A.B., Trottier, Y., Auburger, G., Braak, H. and Schultz, C. (2002) Intranuclear aggregation of nonexpanded ataxin-3 in marinesco bodies of the nonhuman primate substantia nigra. *Exp. Neurol.*, **176**, 117–121.
57. Arrasate, M., Mitra, S., Schweitzer, E.S., Segal, M.R. and Finkbeiner, S. (2004) Inclusion body formation reduces levels of mutant huntingtin and the risk of neuronal death. *Nature*, **431**, 805–810.
58. Perez, M.K., Paulson, H.L. and Pittman, R.N. (1999) Ataxin-3 with an altered conformation that exposes the polyglutamine domain is associated with the nuclear matrix. *Hum. Mol. Genet.*, **8**, 2377–2385.
59. Tait, D., Riccio, M., Sittler, A., Scherzinger, E., Santi, S., Ognibene, A., Maraldi, N.M., Lehrach, H. and Wanker, E.E. (1998) Ataxin-3 is transported into the nucleus and associates with the nuclear matrix. *Hum. Mol. Genet.*, **7**, 991–997.
60. Sun, J., Xu, H., Negi, S., Subramony, S.H. and Hebert, M.D. (2007) Differential effects of polyglutamine proteins on nuclear organization and artificial reporter splicing. *J. Neurosci. Res.*, **85**, 2306–2317.
61. Schmitt, I., Brattig, T., Gossen, M. and Riess, O. (1997) Characterization of the rat spinocerebellar ataxia type 3 gene. *Neurogenetics*, **1**, 103–112.
62. Nijman, S.M., Luna-Vargas, M.P., Velds, A., Brummelkamp, T.R., Dirac, A.M., Sixma, T.K. and Bernards, R. (2005) A genomic and functional inventory of deubiquitinating enzymes. *Cell*, **123**, 773–786.
63. Rodrigues, A.J., Coppola, G., Santos, C., Costa Mdo, C., Ailion, M., Sequeiros, J., Geschwind, D.H. and Maciel, P. (2007) Functional genomics and biochemical characterization of the *C. elegans* orthologue of the Machado–Joseph disease protein ataxin-3. *Faseb. J.*, **21**, 1126–1136.
64. van Bilsen, P.H., Jaspers, L., Lombardi, M.S., Odekerken, J.C., Burright, E.N. and Kaemmerer, W.F. (2008) Identification and allele-specific silencing of the mutant huntingtin allele in Huntington's disease patient-derived fibroblasts. *Hum. Gene. Ther.*, **19**, 710–719.
65. Jarraya, B., Boulet, S., Ralph, G., Jan, C., Bonvento, G., Azzouz, M., Miskin, J., Shin, M., Delzescaux, T., Drouot, X. *et al.* (2009) Dopamine gene therapy for Parkinson's disease in a nonhuman primate without associated dyskinesia. *Sci. Transl. Med.*, **1**, 1–11.
66. de Almeida, L.P., Zala, D., Aebischer, P. and Deglon, N. (2001) Neuroprotective effect of a CNTF-expressing lentiviral vector in the quinolinic acid rat model of Huntington's disease. *Neurobiol. Dis.*, **8**, 433–446.
67. Hottinger, A.F., Azzouz, M., Deglon, N., Aebischer, P. and Zurn, A.D. (2000) Complete and long-term rescue of lesioned adult motoneurons by lentiviral-mediated expression of glial cell line-derived neurotrophic factor in the facial nucleus. *J. Neurosci.*, **20**, 5587–5593.
68. de Almeida, L.P., Ross, C.A., Zala, D., Aebischer, P. and Deglon, N. (2002) Lentiviral-mediated delivery of mutant huntingtin in the striatum of rats induces a selective neuropathology modulated by polyglutamine repeat size, huntingtin expression levels, and protein length. *J. Neurosci.*, **22**, 3473–3483.
69. Livak, K.J. and Schmittgen, T.D. (2001) Analysis of relative gene expression data using real-time quantitative PCR and the 2(-Delta Delta C(T)) Method. *Methods*, **25**, 402–408.
70. Schmued, L.C., Albertson, C. and Slikker, W. Jr (1997) Fluoro-Jade: a novel fluorochrome for the sensitive and reliable histochemical localization of neuronal degeneration. *Brain Res.*, **751**, 37–46.
71. Arango, M., Holbert, S., Zala, D., Brouillet, E., Pearson, J., Regulier, E., Thakur, A.K., Aebischer, P., Wetzel, R., Deglon, N. and Neri, C. (2006) CA150 expression delays striatal cell death in overexpression and knock-in conditions for mutant huntingtin neurotoxicity. *J. Neurosci.*, **26**, 4649–4659.
72. Palfi, S., Brouillet, E., Jarraya, B., Bloch, J., Jan, C., Shin, M., Conde, F., Li, X.J., Aebischer, P., Hantraye, P. and Deglon, N. (2007) Expression of mutated huntingtin fragment in the putamen is sufficient to produce abnormal movement in non-human primates. *Mol. Ther.*, **15**, 1444–1451.
73. Paxinos, G., Watson, C., Pennisi, M. and Topple, A. (1985) Bregma, lambda and the interaural midpoint in stereotaxic surgery with rats of different sex, strain and weight. *J. Neurosci. Methods*, **13**, 139–143.
74. Clarke, P.G. (1992) How inaccurate is the Abercrombie correction factor for cell counts? *Trends Neurosci.*, **15**, 211–212.